



# Improvement of the RF cavity for the SKKUCY-10 cyclotron

Jongchul Lee<sup>1,2</sup> · Mitra Ghergherehchi<sup>3</sup> · Khaled M. M. Gad<sup>1</sup> · Donghyup Ha<sup>3</sup> · Ho Namgoong<sup>3</sup> ·  
Seunghyun Lee<sup>4</sup> · Ho Seung Song<sup>3</sup> · Berat Can Karatas<sup>3</sup> · Jong-Seo Chai<sup>3</sup>

Received: 16 February 2021 / Revised: 16 April 2021 / Accepted: 27 April 2021 / Published online: 25 October 2021  
© The Korean Physical Society 2021

## Abstract

The SKKUCY-10 cyclotron based on 83.2 MHz, 40 kV half-wave RF cavity was developed at Sungkyunkwan University for the production of medical radioisotopes. The resonant frequency  $f_{RF}$  of the cyclotron and the RF coupling coefficient  $\beta_c$  of the RF cavity system were measured at various vacuum, and temperature conditions. The normalized multi-pacting intensities at four positions in the power coupler were analyzed to predict the multi-pacting power. Differences,  $\Delta f_{RF}$  and  $\Delta \beta_c$ , caused by the vacuum, and temperature conditions were modified based on the coupler and tuner gap distances. During the RF conditioning, a constant 15 kW pulse mode and a variable 1 to 15 kW continuous wave mode were employed. The values of the reflection coefficient  $\Gamma$  and  $\beta_c$  were 1.2% and 0.8, respectively, when the cavity dissipation power was 12.4 kW at 83.2 MHz. Good agreement between the simulation and experimental data was obtained.

**Keywords** RF cavity · Cyclotron · Resonant frequency · Coupling coefficient · RF conditioning

## 1 Introduction

The cyclotron was developed to accelerate charged particles and has been used to produce radioisotopes for medical applications. The cyclotron RF cavity system, which consists of a dee (for an electric field), power coupler (for the transmission of RF power), and fine tuner (for a constant resonant frequency), was developed to generate an accelerating electric field [1]. The resonant frequency ( $f_{RF}$ ) of the cyclotron, which is in the range of a few tens of MHz, is selected by considering the harmonic number, magnetic field, particle species, and the structure of the RF cavity [2–5].

Because of the phase difference between the particle orbit and RF electric field,  $f_{RF}$  is designed carefully through the RF cavity [6]. However, the resonant frequency can be

altered due to a fabrication error, as well as vacuum pressure, and temperature variations, and for constant  $f_{RF}$ , an RF cavity was developed using one or two capacitive fine tuners [7]. Two power couplers, inductive and capacitive coupling types, have been developed for the transmission of the RF power and minimization of the reflected power from the power coupler to the RF cavity [8, 9]. The main advantage of electric field coupling is that it has less impact on the multi-pacting effect compared to magnetic field coupling [10]; therefore, capacitive coupling is used in our design.

The 10 MeV cyclotron (SKKUCY-10) [11] based on the 83.2 MHz, 40 kV half-wave RF cavity was fabricated for the production of the medical radioisotope <sup>18</sup>F ( $t_{1/2} = 109$  min) used in positron emission tomography (PET) [12]. The design of the RF cavity was considered to improve the energy gain, and the quality factor, so the RF cavity geometry was optimized to increase the unloaded quality factor ( $Q_0$ ) 5830 and to decrease the cavity dissipation power ( $P_c$ ) 12.4 kW [13].

A capacitive power coupler and fine tuner were installed in the vacuum chamber, and the characteristic impedance (50  $\Omega$ ) and tunable RF frequency ( $\pm 0.5$  MHz) were measured by using a network analyzer. When the high RF power is input to the RF cavity, the vacuum condition and magnetic field need to be prepared. Therefore, the RF characteristics may vary due

✉ Jong-Seo Chai  
jschai@skku.edu

<sup>1</sup> WCU Department of Energy Science, Sungkyunkwan University, Suwon, Republic of Korea  
<sup>2</sup> Advanced Radiation Technology Institute, Korea Atomic Energy Research Institute, Jeongeup, Republic of Korea  
<sup>3</sup> College of Information & Communication Engineering, Sungkyunkwan University, Suwon-si, Republic of Korea  
<sup>4</sup> Korea Atomic Energy Research Institute, Daejeon, Republic of Korea

to the vacuum, and temperature conditions caused by the magnetic coil and RF power.

## 2 Methods and materials

### 2.1 RF cavity system

The vertical half-wave RF cavity of the 10-MeV cyclotron was designed with two dees and consisted of a power coupler and a fine tuner. The main design specifications are listed in Table 1. The 12.4 kW cavity dissipation power of a RF cavity was required for a 40 kV dee voltage; therefore, a 20 kW solid-state RF amplifier was developed [14]. By combining eight modules (3.2 kW), the desired RF power could be amplified, and an absorption resistor was implanted in each module to protect it from the damage caused by the reflected power. The RF signal can be generated using a signal generator with both pulse and continuous wave modes and amplified by increasing the bias voltage.

### 2.2 Theoretical approach to the RF characteristics Dee configuration of the RF cavity

The desired RF values of the resonant frequency ( $f_{\text{RF}} = 83.2$  MHz) and the coupling coefficient ( $\beta_c = 1$ ) depend on the RF operating conditions, so these parameters should be optimized to avoid damage to the RF amplifier and the cavity system. The vacuum and temperature conditions were investigated for the RF operating conditions to find desirable RF values during the RF conditioning process, and the vacuum and temperature conditions were applied from the settings of air and room temperature, respectively. The  $f_{\text{RF}}$  relation between air and vacuum can be expressed as Eq. (1),

$$\frac{1}{\lambda_0 \sqrt{\epsilon_0 \mu_0}} = f_{\text{RF, vacuum}} = f_{\text{RF, air}} \sqrt{\epsilon_r}, \quad (1)$$

where  $\epsilon_0$ ,  $\mu_0$ ,  $\lambda_0$  are the permittivity, permeability, wavelength in vacuum, respectively, and  $\epsilon_r$  is the relative permittivity in air [15]. Moreover, the coil current of the magnet

and the ohmic loss of the dissipated cavity power increase the total temperature of cyclotron; therefore,  $f_{\text{RF}}$  and  $\beta_c$  can be increased, as well. The frequency difference  $\Delta f_{\text{RF}}$  was denoted as  $\Delta f_{\text{RF}} = -f_{\text{RF}}(\Delta L/L)$ , where  $L$  is the linear dimension of the cavity, and  $\Delta L/L$  was studied for oxygen-free copper [16].

Meanwhile, the value of  $\beta_c$  between the power coupler and RF cavity can be represented as,

$$\beta_c = \frac{P_e}{P_c} = \frac{2P_e}{R_s \int H^2 dS}, \quad (2)$$

where  $P_c$  and  $P_e$  are the cavity dissipation power and external power, respectively [17]. The cavity dissipation power alters the RF surface resistance ( $R_s$ ), which can be presented in terms of the temperature resistivity ( $\rho_{T2} = \rho_{T1}(1 + \beta_T(T_2 - T_1))$ ) and the skin depth ( $\delta$ ) of oxygen-free copper, where  $\rho_{T1}$  is the resistivity at the initial temperature and  $\beta_T$  is the temperature coefficient  $1/(233.54 + T)$  for copper [18].

### 2.3 Power coupler and fine tuner for RF tuning

Figure 1 shows, the designed power coupler, fine tuner, and pick-up probe with detailed components are manufactured. The position of the coupler plate is fixed; however, that of the tuner plate can be moved using a stepping motor. The power coupler has cooling channels, which were manufactured using polyether ether ketone (PEEK) as insulation between the inner and the outer conductors. The rod for the pick-up probe was designed with consideration of the coupling attenuation due to the dee.

The multi-pacting effect is a major issue in generating reflected RF power during the RF conditioning, regardless of the cyclotron RF cavity. However, the power coupler is connected to the RF amplifier, even if the magnetic field is negligible, and the multi-pacting effect was analyzed using a power coupler simulation. In our RF system, the power coupler was designed based on a coaxial waveguide with a characteristic impedance ( $Z_0$ ) of 50  $\Omega$  and a multi-pacting power ( $P_m$ ) of the coaxial waveguide, which can be expressed as,

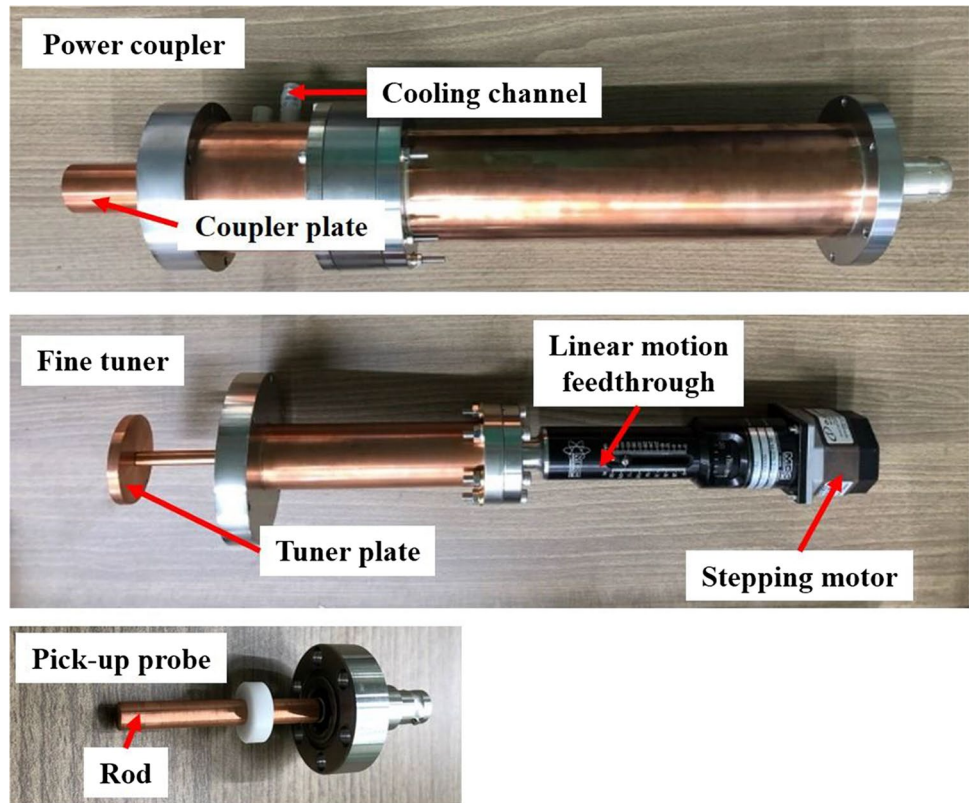
$$P_m = \frac{A\omega^4(r_2 - r_1)^4 m^2}{\pi\eta e^2 \ln(r_2/r_1)}, \quad (3)$$

where  $A$  has the constant value of 0.25 for a traveling wave,  $\omega = 2\pi f_{\text{RF}}$  is the RF angular frequency,  $r_1$  and  $r_2$  are the inner/outer conductor radii of the coaxial waveguide,  $\eta$ ,  $m$  and  $e$  are the wave impedance in vacuum, electron mass and charge, respectively [19]. The detailed structure of the power coupler was evaluated for the multi-pacting power condition using the CST-Particle Studio code through the RF eigenmode [20]. Additionally, the static magnetic field that was generated by the cyclotron magnet was imported,

**Table 1** RF cavity parameters for the 10 MeV Cyclotron

Design parameter	
Resonant frequency (MHz)	83.2
Resonant structure	$\lambda/2$
Dee voltage (kV)	40
Cavity dissipation power (kW)	12.4
Characteristic impedance ( $\Omega$ )	50
Coupler type	Capacitive coupling
Frequency tuning range (MHz)	$\pm 0.5$
Amplifier type	Solid-state
Maximum output RF power (kW)	20

**Fig. 1** Manufactured power coupler, fine tuner, and pick-up probe



and four initial electron positions (positions 1–4) near the RF window and adaptor are shown in Fig. 2.

### 3 Experimental results

Optimizations of the resonant frequency ( $f_{RF}$ ), RF coupling coefficient ( $\beta_c$ ), and performance of the RF conditioning were performed through analyses of experimental data. The components of the 10 MeV cyclotron are

shown in Fig. 3. The RF cavity was installed inside the vacuum chamber, and the power coupler and the fine tuner are located on the right/left sides of the vacuum chamber, respectively. The penning ionization gauge (PIG) ion source is positioned at the center of the cyclotron, and it can be moved in the horizontal plane. The vacuum system comprises two rotary and diffusion pumps. The magnet power supply (MPS), and a solid-state RF amplifier are connected to the coil and the power coupler, respectively.

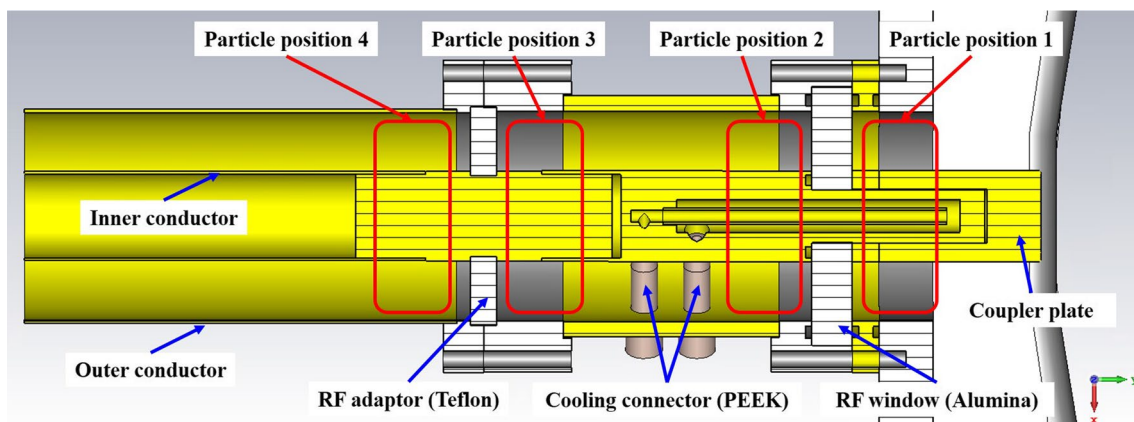


**Fig. 2** Detailed scheme of the power coupler for multi-pacting simulation

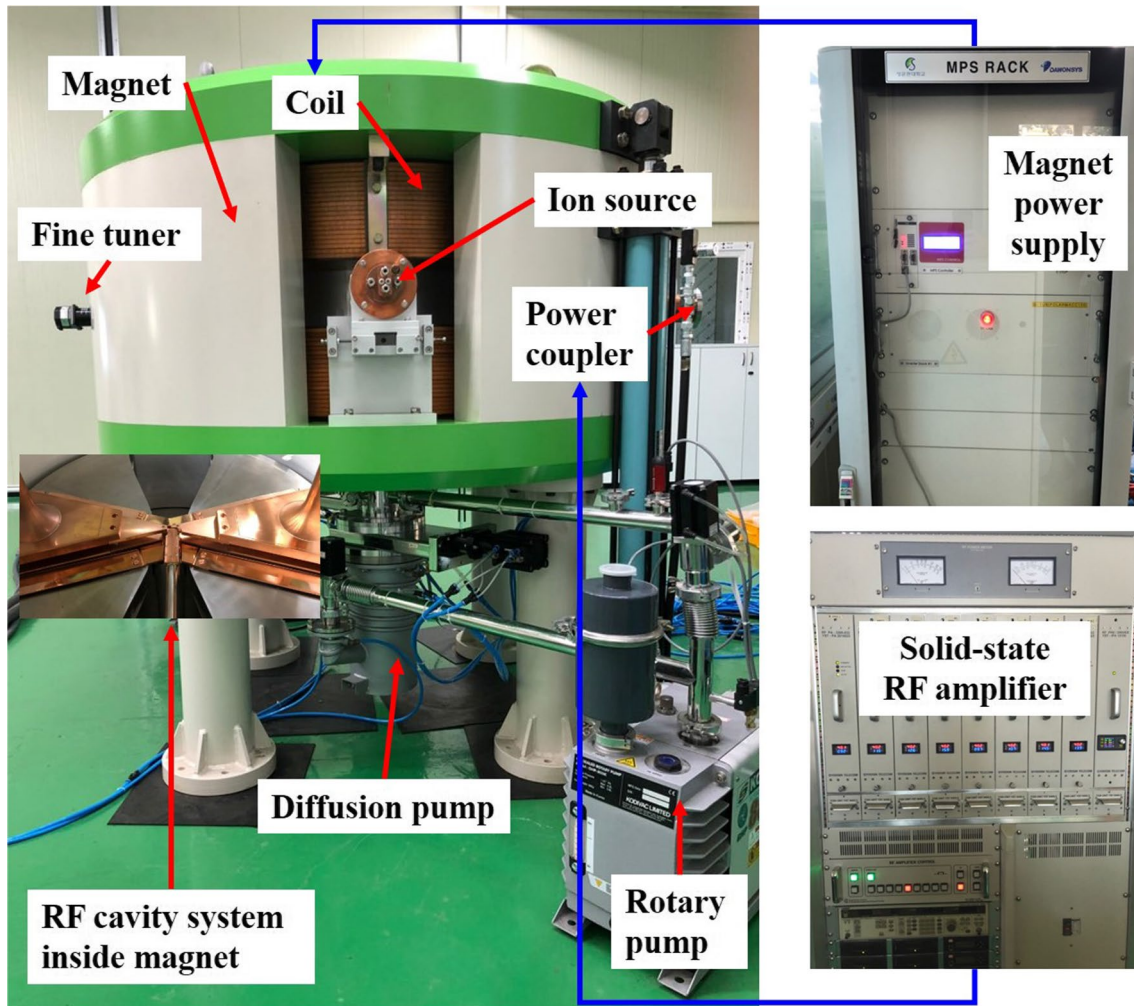


Fig. 3 10 MeV cyclotron system with a magnet power supply and a solid-state RF amplifier

### 3.1 Tuning results for the frequency and coupling coefficient

The  $f_{\text{RF}}$  and  $\beta_c$  were measured using a network analyzer under various conditions of vacuum and temperature, relative to the reference values ( $f_{\text{RF}} = 83.2$  MHz,  $\beta_c = 1.03$ ). The calculated and the measured RF characteristics are listed in Table 2. At first, the RF characteristics were measured by applying each condition (vacuum, temperature), after which two conditions (net conditions) were applied together in the RF cavity.

The  $\Delta f_{\text{RF}} (= f'_{\text{RF}} - f_{\text{RF}})$  values were calculated based on the difference between  $f'_{\text{RF}}$  (Eq. 1) and the reference data, and the  $\Delta\beta_c$  values were calculated using the frequency ratio ( $f'_{\text{RF}}/f_{\text{RF}}$ ) with a relative permittivity of 1.000647 in air. Meanwhile, for a coil current of 242.2 A, the room temperature was increased to 40 °C inside the RF cavity. The statistic of error in  $\Delta f_{\text{RF}}$  between the calculated and the measured values was less than 8%; however, the  $\Delta\beta_c$  error

Table 2 RF Characteristics corresponding to various vacuum and temperature conditions

Design parameter	Vacuum condition	Temperature condition	Net condition*
$\Delta f_{\text{RF}}[\text{kHz}]$ (Calc.)	26.9	27.6	54.5
$\Delta f_{\text{RF}}[\text{kHz}]$ (Meas.)	27	32	59
$\Delta\beta_c$ (Calc.)	0.0003	0.04	0.00403
$\Delta\beta_c$ (Meas.)	0.03	0.16	0.19

was 98%. A significant portion of the  $\Delta\beta_c$  error was caused by the external power ( $P_e$ ) and the increase in the temperature, which could not be approximated in the calculation; to overcome this problem, we had to re-optimize  $\beta_c$ .

$\Delta f_{\text{RF}}$  and  $\Delta\beta_c$  were optimized by considering the design of the power coupler apparatus. Figure 4 shows the simulated and the measured results according to the power coupler gap distance. When the gap distance was increased,  $\Delta f_{\text{RF}}$

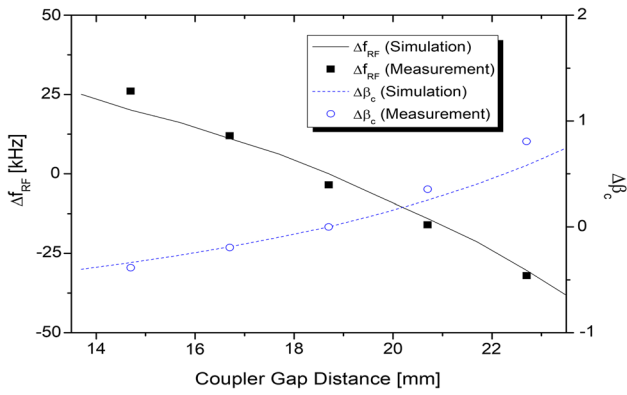


Fig. 4  $\Delta f_{RF}$  and  $\Delta\beta_c$  vs. coupler gap distance

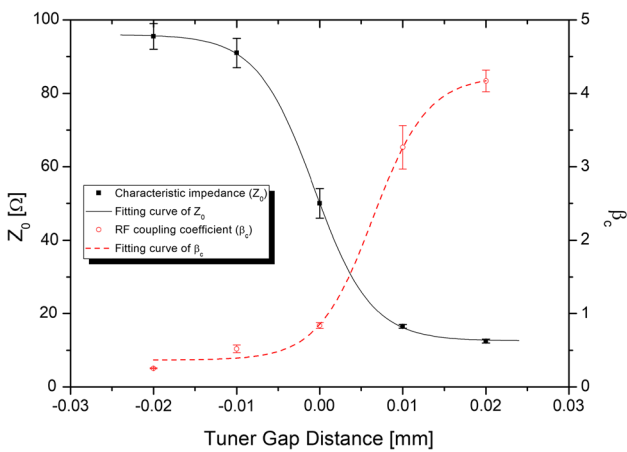


Fig. 5 Measurement results for the characteristic impedance and coupling coefficient vs. to tuner gap distance

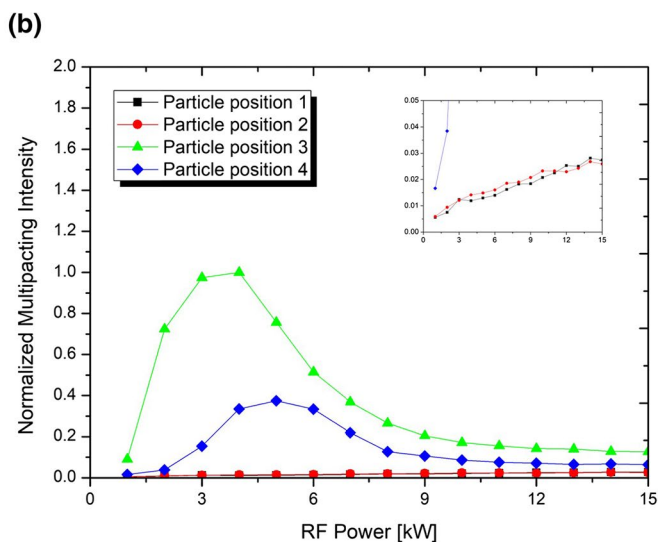
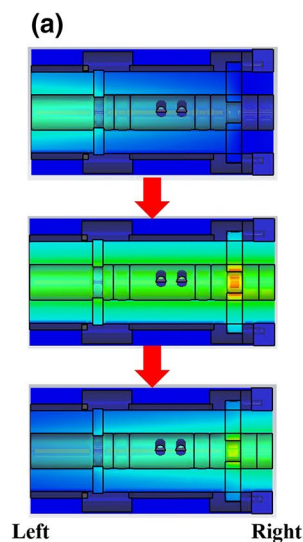
decreased because the applied electric field introduced an additional capacitance between the power coupler and the dee whereas  $\Delta\beta_c$  increased because the external power ( $P_e$ ) was increased according to Eq. (2). The characteristic impedance ( $Z_0$ ) and coupling coefficient ( $\beta_c$ ) corresponding to the tuner gap distance were measured at  $f_{RF} = 83.2$  MHz, and the results are shown in Fig. 5.  $\beta_c$  increased and  $Z_0$  decreased with increasing tuner gap distance via decreasing the cavity dissipation power ( $P_c$ ).

### 3.2 Results for the power coupler, pick-up probe, fine tuner

The multi-pacting power was considered in the design of the power coupler, which has high possibility of RF reflection, to predict the power level; the theoretical calculation and the simulation results were compared using a coaxial waveguide in the CST-PS PIC code [21]. Figure 6a shows the RF magnetic field distribution, which is a TEM mode in the traveling wave mode. The magnetic field in the traveling wave mode depend on time (according to the RF period) and generated a field from the RF amplifier (Left) to the cavity (Right). Figure 6b shows the normalized multi-pacting intensity (ratio of the number of secondary electrons to the highest value of secondary electrons) vs. the RF power. In the figures the particle intensities for positions 1 and 2 were almost negligible because of the static magnetic field.

The multi-pacting power ( $P_m$ ) of the coaxial waveguide were obtained as 2.2 kW and 4 kW using calculations based on Eq. (3) and a simulation at position 3 of the power coupler, respectively. The effect of the multi-pacting intensity at position 4 was less than that at position 3, owing to the geometry of the power coupler. The normalized multi-pacting intensity was 0.12 kW at the desired cavity dissipation power ( $P_c = 12.4$  kW) at position 3.

Fig. 6 a Magnetic field distribution in the traveling wave mode and b normalized multi-pacting intensity vs. the RF power



The cyclotron RF experimental setup is shown in Fig. 7. In the block diagram, the RF signals are measured through forward ( $V_f$ ) and reflected ( $V_r$ ) voltages and the transmitted RF power ( $P_t$ ).

The experiment was performed at a vacuum pressure of  $3 \times 10^{-6}$  mbar, a coil current of 242.2 A, and a coil temperature of 29 °C, as shown in Fig. 8. A 15 kW traveling wave RF power with a pulse width of 10  $\mu$ s and a repetition rate of 200 Hz were applied in the RF conditioning process.

The reflection coefficient ( $\Gamma$ ) was calculated by measuring the forward and the reflected voltages ( $V_f$ ,  $V_r$ ) via DC connectors, and the vacuum pressure was measured using a vacuum gauge. When the pulse width was

increased to 1500  $\mu$ s, the vacuum pressure remained less than  $4.4 \times 10^{-6}$  mbar; however,  $\Gamma$  fluctuated because of the increased average cavity dissipation power in the RF cavity with increasing pulse width.

Figure 9 shows the measurement results for the RF characteristics ( $\beta_c$ ,  $P_c$ ) and the reflection coefficient ( $\Gamma$ ) in the continuous wave mode based on the (a) RF input power and (b) the tuning gap distance, respectively. When the RF input power was increased,  $\beta_c$  decreased owing to the increase in the temperature inside the RF cavity; for the optimal value of  $\beta_c = 1$ , we could achieve a cavity dissipation power of 12.4 kW at an RF input power of 12.55 kW by interpolation.

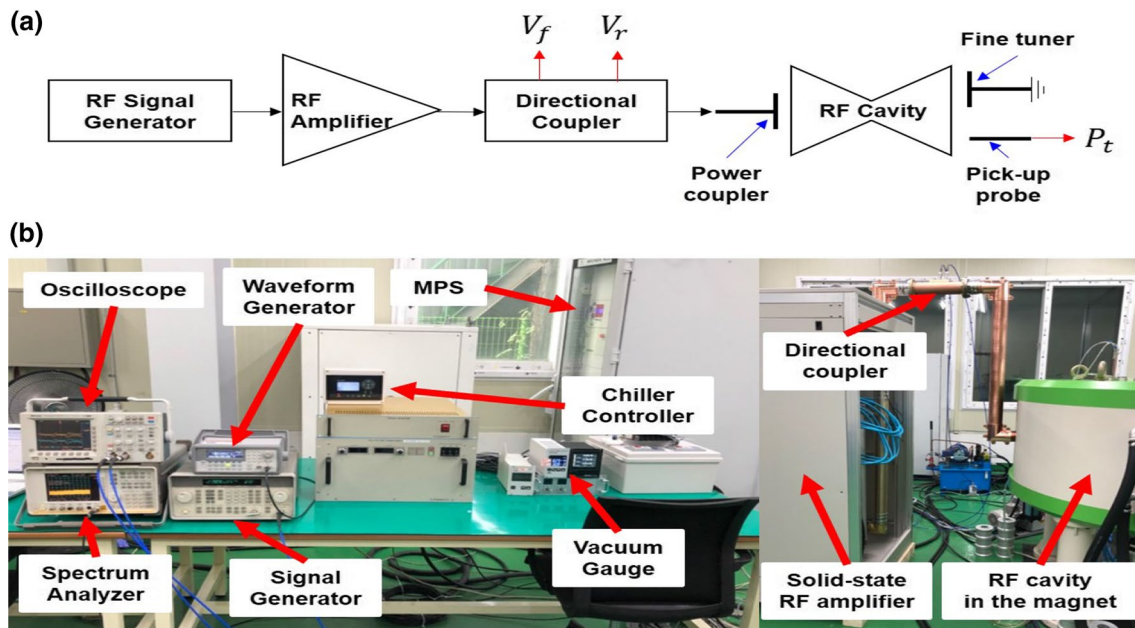


Fig. 7 Experimental setup for RF conditioning

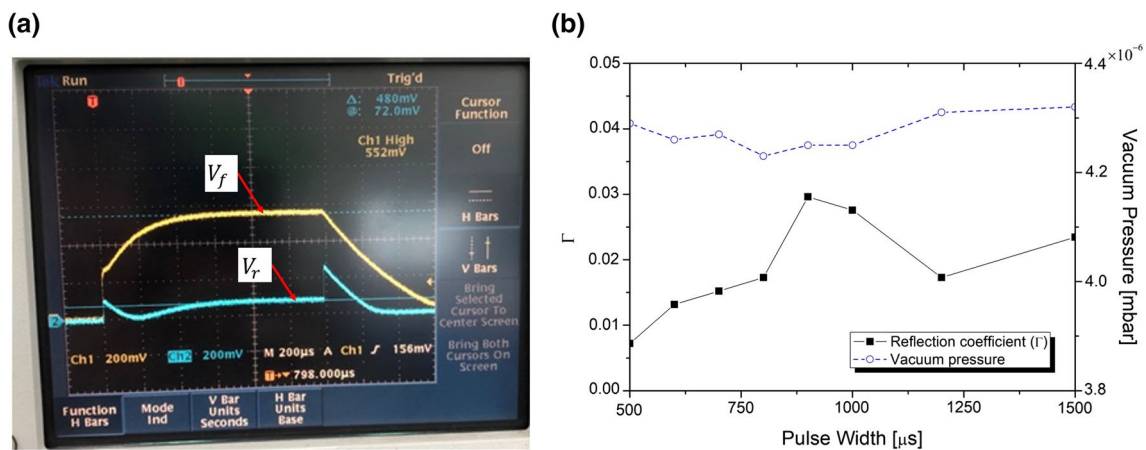
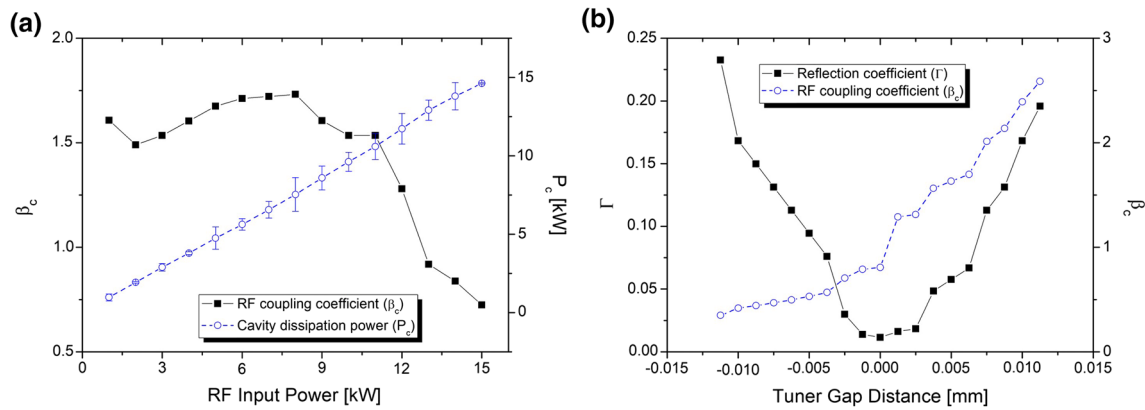


Fig. 8 Experimental setup: **a** forward and reflected voltage and **b**  $\Gamma$  vs. pulse width



**Fig. 9** Measurement results for the RF characteristics vs. **a** the RF input power and **b** the tuning distance at a 12.4 kW cavity dissipation power

Figure 9b shows a semi-symmetric exponential behavior of  $\Gamma$  versus the tuner gap distance at the maximum cavity dissipation power of 12.4-kW. When the tuner gap distance was increased,  $\beta_c$  increased, and tuner gap distance was adjusted to obtain the optimum  $\beta_c = 1$  using a stepping motor with a step size in the 0.0125 mm range.  $\beta_c$  were measured as 0.806 and 1.29 at 0 mm and 0.0125 mm tuner gap distance, respectively; as a result, the critical coupled state ( $\beta_c = 1$ ) was obtained by interpolation.

## 4 Discussion and conclusion

Optimizations of the resonant frequency ( $f_{RF}$ ), RF coupling coefficient ( $\beta_c$ ), performance of the RF conditioning, and the 12.4 kW cavity dissipation power ( $P_c$ ) were tested through experimental procedures. The multi-pacting effect was considered for the coaxial waveguide power coupler, and the multi-pacting power was simulated as 4 kW in the traveling wave mode. The constant 15 kW pulse mode and the variable 1–15 kW continuous mode were employed during the RF conditioning. The obtained reflection coefficient ( $\Gamma$ ) and  $\beta_c$  values were 1.2% and 0.8, respectively, at  $f_{RF} = 83.2$  MHz, and  $P_c = 12.4$  kW. The RF control system can automatically be applied for a stable RF operation, dee voltage, and resonant frequency using RF feedback control, including an RF amplifier and a fine tuner, as future work.

**Acknowledgements** This work was supported by the Radiation Technology R&D program through the National Research Foundation of Korea funded by the Ministry of Science, ICT & Future Planning (2017M2A2A4A02020347).

## References

1. P.K. Sigg, CERN-2006-012, RF for cyclotrons, Zeegse, The Netherlands (2006).

2. V. Smirnov, S. Vorozhtsov, Phys. Part. Nucl. **47**, 683 (2016)
3. G. Gold et al., in *Design of a Digital Low-Level RF System for Best Medical Cyclotrons*, Proceedings of CYCLTRONS, Canada (2013).
4. I.S. Jung et al., in *Design of The RF System for a 30 MeV Cyclotron*, Proceedings of EPAC, Edinburgh, Scotland (2006).
5. Z. Yin et al., Nucl. Instrum. Methods A. **854**, 25 (2017)
6. K. Strijckmans, Comput. Med. Imaging Graph. **25**, 69 (2001)
7. Z.G. Yin et al., Nucl. Instrum. Methods A. **921**, 38 (2019)
8. L. Carroll, Phys. Proc. **90**, 126 (2017)
9. G. Liu et al., Nucl. Instrum. Methods A. **908**, 143 (2018)
10. P.K. Sigg, *Cyclotron Cavities, Part 2* (Paul Scherrer Institute, Villigen, 2003)
11. J. Lee et al., Nucl. Instrum. Methods B. **468**, 71 (2020)
12. S. Oh et al., Appl. Radiat. Isot. **131**, 23 (2018)
13. J. Lee et al., Nucl. Instrum. Methods A. **939**, 66 (2019)
14. H.S. Song et al., IEEE Trans. Nucl. Sci. **66**, 1924 (2019)
15. M.E.V. Valkenburg, *Reference Data for Engineers: Radio, Electronics, Computer, and Communications* (Elsevier, Amsterdam, 2002)
16. P. Zhang et al., Nucl. Instrum. Methods A. **797**, 101 (2015)
17. T.P. Wangler, *RF Linear Accelerators* (Wiley, Hoboken, 2008)
18. C.D. Association, *High Conductivity Coppers* (CDA Publication, California, 1998)
19. Z. Zheng et al., Nucl. Instrum. Methods A. **735**, 596 (2014)
20. CST Particle Studio, 3DS Dassault Systems Simulia (2021). <https://www.3ds.com>
21. M.A. Furman, M.T.F. Pivi, *Probabilistic Model for the Simulation of Secondary Electron Emission* (Lawrence Berkeley National Laboratory, California, 2003)

**Publisher's Note** Springer Nature remains neutral with regard to jurisdictional claims in published maps and institutional affiliations.